About the collapse of the 3.3 μm CH stretching band with ionization in polycyclic aromatic hydrocarbons: Configuration interaction and quantum Monte Carlo studies of the CH fragment

Françoise Pauzat, Julien Pilmé, Julien Toulouse, Yves Ellinger

About the collapse of the 3.3μm CH stretching band with ionization in PAHs: Configuration Interaction and Quantum Monte Carlo studies of the CH fragment

Françoise Pauzat,[1] Julien Pilmé,[1,2] Julien Toulouse,[1] Yves Ellinger[11, a)]

[1] *UPMC Univ Paris 06, CNRS - UMR 7616, Laboratoire de Chimie Théorique, Paris, France.*

[2] *Faculté de Pharmacie, Univ Lyon 1, Lyon, France.*

(Dated: 21 June 2010)

The puzzling difference between the IR spectra of polycyclic aromatic hydrocarbons (PAHs) and those of the corresponding positive ions ($PAHs^+$) is a well documented fact, although the basic reason for it is far from clear. In this report, the CH fragment, in its neutral and ionized forms is taken as a case study for investigating the collapse of the CH stretching vibration with ionization. A comprehensive study of the dipole moment function around the equilibrium geometries of the fragments using large scale configuration interaction and quantum Monte Carlo methods shows very different variations with the CH distance: a marked decrease for neutral $CH(^2\Pi)$ and a perfect stability for ionized $CH^+(^1\Sigma^+)$. These results are consistent with strong/weak intensities of the CH vibrations in the neutral/ionized PAHs, the key point being the presence, or not, of a hole in the π shell. A topological analysis of the electronic densities shows that the collapse of the CH stretching with ionization is directly linked to the compensation between the internal charge transfer contribution and the distortion of the electronic density within the CH bond.

[a)] Electronic mail: pauzat, pilme, toulouse, ellinger@lct.jussieu.fr

I. INTRODUCTION

The suggestion that polycyclic aromatic hydrocarbons (PAHs) were the carriers of the unidentified infrared (UIR) bands[1,2] has motivated considerable efforts from the astrophysics community. The 3.3 μm band of the UIR spectra whose intensity varies drastically from one astrophysical object to another has probably been the feature subject to the most specific theoretical as well as experimental investigations. One of the most surprising results of these first investigations was that the IR spectra of the positive ions ($PAHs^+$) at 3.3 μm presented a total collapse in the band intensities with ionization[3–11]. Such a collapse was certainly not expected in view of the marginal geometric modifications with respect to the neutral parents. Although an increasing number of theoretical spectra of PAHs are routinely available to day in databases[12,13] and high level theoretical works are carried out to establish the importance of PAHs radical cations in the interstellar clouds[14–19], the basic reason at the origin of this seemingly widely spread phenomenon in the PAHs population has never been really clarified.

The collapse of the CH stretching with ionization is certainly a robust fact for *genuine* PAHs. First predicted[3] and observed in the laboratory for naphthalene[4] anthracene[6] and pyrene[7], it has been confirmed and shown to persist for much larger linear and compact PAHs[10,11].The electronic structure of these species is well represented by naphthalene (FIG.1) in the neutral (**I**) and ionized (**II**) forms. Structure (**I**) is typical of singlet aromatic compounds with a complete π shell where each carbon atom gives a 2p electron to the delocalized system; structure (**II**) is the corresponding positive ion where one electron has been removed from the π shell, so that there is one less π electron than the number of carbon atoms. The IR stretching vibration is very strong for the neutral whereas it is very weak (between one and two orders of magnitude less) in the ionized species.

However, PAHs are not necessarily built of condensed six-membered rings. We have considered that irregular structures incorporating even-membered rings are possible and can be well represented by the fluorenyl radical (FIG.1). In structure (**III**), the neutral system is an open-shell of doublet multiplicity with a complete π shell. Structure (**IV**) is the corresponding positive ion; contrary to naphthalene, the positive ion is a singlet state that has also one less π electron than the number of carbon atoms. Again the IR stretching vibration is found very strong for neutral fluorenyl whereas it is very weak for the cation[20].

The possibility that PAHs are slightly dehydrogenated in space has also to be considered[21]. Such a situation is represented by dehydrogenated naphthalene (FIG. 1). In structure (**V**), a hydrogen atom has been removed in the α position ; the PAH remains neutral with a complete π shell and a σ dangling orbital containing an unpaired electron (doublet state). Ionization leads to two different ions according as the electron is removed from the localized dangling orbital or from the delocalized system. In structure (**VI**), the electron is removed from the delocalized system; it is an open-shell triplet with one less π electron than the number of carbon atoms; the IR stretching vibration is very weak. In structure (**VII**), the positive charge is localized in the aromatic plane on the α carbon; it is a closed shell singlet with a complete π shell. Here we found the puzzling result that, for both species, the neutral as well as the ionized, the IR stretching vibration is very strong. Removing a β hydrogen leads to the same conclusions[22].

The conclusion that can be drawn from the body of data gathered on different types of PAHs is that ionization is certainly not the only factor leading to the collapse of the CH stretching vibration; neither is the spin multiplicity, nor the charge of the PAH. *The only common point is the presence of a hole in the π shell.*

Looking for the basic reason at the origin of the phenomenon is the main goal of this report. All theoretical and experimental studies of PAHs have shown that the CH stretching vibration is well separated from the other vibrations; it is a local mode, not coupled with the other motions of the nuclei, which suggests that the CH fragment can be considered as model for a case study (FIG. 2). The neutral fragment CH, in its ground state $^2\Pi$, with one π electron on one carbon, is a model for structures **I**, **III** and **V**. The ionized fragment CH^+ in its ground state $^1\Sigma^+$ with no π electron on carbon, i.e. a hole in the π system is a model for structures **II** and **IV** and **VI**, whereas CH^+ in its excited state $^3\Pi$ presents the same situation as structure **VII** with a positive charge in the σ system and a complete π shell.

Since the IR intensities scale with the square of the derivative of the dipole moment associated with the displacement of the nuclei, we calculated the electric dipole moments of the CH fragment in its ground state $^2\Pi$ and CH^+ in its ground state $^1\Sigma^+$ and first excited state $^3\Pi$, using the multi-reference configuration interaction (MRCISD) method with single and double excitations, as well as quantum Monte Carlo (QMC) approaches developped recently in our laboratory. Anticipating further calculations on larger PAHs, we also verified

that density functional theory (DFT) gives analoguous answers.

The present report is organized as follows. In section 2 we present the main characteristics of the theoretical methods used and we show that the results of these very different approaches agree well with each other and with other levels of calculations[11], which gives us confidence in their accuracy. A topological analysis of the B3LYP density based on the Electron Localization Function (ELF) is developped in section 3 for interpreting the variation of the dipole moment with the CH elongation. Conclusions are given in section 4.

II. ACCURATE CALCULATIONS OF DIPOLE MOMENTS

For non-neutral systems such as CH^+, the electric dipole moment is origin dependent. Here, it was calculated with respect to the center of mass, which is relevant for rotational/vibrational spectroscopies that probe the system in its center-of-mass reference frame. In these conditions, the dipole moment is written as the sum of nuclear and electronic contributions, $\boldsymbol{\mu} = \boldsymbol{\mu}^n + \boldsymbol{\mu}^e$, with $\boldsymbol{\mu}^n = \sum_a Z_a \mathbf{R}_a$ (where the sum is over all nuclei a of charges Z_a and located at $\mathbf{R}_a$).

A. MRCISD calculations

We perform multiconfiguration self-consistent-field (MCSCF) calculations with complete active spaces (CAS) generated by distributing n electrons in m orbitals [CAS(n,m)], followed by MRCISD calculations taking the full CAS as reference space. We have tested full valence active spaces, i.e. CAS(5,5) for CH and CAS(4,5) for CH^+, and full core+valence active spaces, i.e. CAS(7,6) for CH and CAS(6,6) for CH^+. Including the $1s$ core electrons in the active space results in an increase of the dipole moments by at most 0.01 Debye. The basis used is cc-pVQZ.

B. QMC calculations

As QMC calculations of dipole moments are less standard we give here more details.

We start by generating a MCSCF wave function with a full valence CAS using the quantum chemistry program GAMESS[23]. We use the CVB2 Slater basis of Ema *et al.*[24],

each Slater function being actually approximated by a fit to 14 Gaussian functions[25–29] in GAMESS.

This standard *ab initio* wave function is then multiplied by a flexible Jastrow factor consisting of the exponential of the sum of electron-nucleus, electron-electron and electron-electron-nucleus terms, written as systematic polynomial and Padé expansions[30] (see also Refs. 31 and 32). Some parameters are fixed by imposing cusp conditions on the wave function, and essentially all other free parameters are chosen to be initially zero to form our starting trial Jastrow-Slater wave function. The QMC calculations are performed with the program CHAMP[33] using the true Slater basis set rather than its Gaussian expansion. The Jastrow, CSF, orbital parameters are simultaneously optimized with the recently-developed linear energy minimization method[34–36] in variational Monte Carlo (VMC), using an accelerated Metropolis algorithm[37,38]. We use an energy convergence threshold of 10^{-4} Ha. Once the optimized trial wave function $\Psi(\mathbf{R})$ has been obtained, we calculate the dipole moment in variational and diffusion Monte Carlo (DMC). The DMC calculations are done within the short-time and fixed-node (FN) approximations (see, e.g., Refs. 39–43). We use an imaginary time step of $\tau = 0.01$ Ha^{-1} in an efficient DMC algorithm featuring very small time-step errors[44].

We compute the electronic dipole moment in QMC using the straightforward local estimator

$$\boldsymbol{\mu}_L^e(\mathbf{R}) = -\sum_{i=1}^{N} \mathbf{r}_i \tag{1}$$

where $\mathbf{R} = (\mathbf{r}_1, \mathbf{r}_2, \cdots, \mathbf{r}_N)$ designates the N electron coordinates. The VMC estimate of the dipole moment is given by the average of this estimator over M electron configurations $\mathbf{R}_k$ distributed according to the probability density $\Psi(\mathbf{R})^2$

$$\boldsymbol{\mu}^e_{\mathrm{VMC}} = \frac{1}{M}\sum_{k=1}^{M} \boldsymbol{\mu}_L^e(\mathbf{R}_k) = \langle \boldsymbol{\mu}_L^e(\mathbf{R}) \rangle_{\Psi^2} \,. \tag{2}$$

In DMC, the dipole moment is calculated as the average of the local estimator over the mixed distribution $\Psi_{\mathrm{FN}}(\mathbf{R})\Psi(\mathbf{R})$ where $\Psi_{\mathrm{FN}}(\mathbf{R})$ is the fixed-node wave function

$$\boldsymbol{\mu}^e_{\mathrm{DMC}} = \langle \boldsymbol{\mu}_L^e(\mathbf{R}) \rangle_{\Psi_{\mathrm{FN}}\Psi} \,. \tag{3}$$

The systematic bias in the VMC estimate of the dipole moment $\boldsymbol{\mu}^e_{\mathrm{VMC}}$ vanishes only linearly with respect to the error in the wave function $\delta\Psi = \Psi - \Psi_0$ (where Ψ_0 is the exact

wave function), in contrast with the case of the total energy which is quadratic with $\delta\Psi$. Similarly, the systematic bias in the DMC estimate $\boldsymbol{\mu}^e_{\rm DMC}$ is linear with respect to both $\delta\Psi$ and $\delta\Psi_{\rm FN} = \Psi_{\rm FN} - \Psi_0$, the error in the fixed-node wave function. Consequently, the calculated dipole moments are much more sensitive to the quality of the wave function than the total energy is. The better hybrid "2DMC-VMC" estimate

$$\boldsymbol{\mu}^e_{\rm hybrid} = 2\boldsymbol{\mu}^e_{\rm DMC} - \boldsymbol{\mu}^e_{\rm VMC} \tag{4}$$

has a systematic bias which is still linear in $\delta\Psi_{\rm FN}$ but now quadratic in $\delta\Psi$, and it is thus much less sensitive to the quality of the wave function.

We now discuss several limitations to the accuracy of the QMC calculations of dipole moments, taking the CH molecule as a test example. A first obvious limitation is the statistical uncertainty on the calculated value of the dipole moment which is inherent to Monte Carlo approaches and directly related to the variance of the estimator of Eq. (1). The relative statistical uncertainty on the dipole moment is much bigger than the relative statistical uncertainty on the total energy. Although improved estimators with reduced variances can be constructed (e.g., similarly to what has been done in Ref. 45), in practice for the small systems studied here, one can easily perform sufficiently long Monte Carlo runs to obtain acceptably small statistical uncertainties. We use Monte Carlo samples of sizes of the order of $M \sim 10^8$ giving statistical uncertainties of about 0.001 Debye in VMC, 0.003 Debye in DMC and 0.006 Debye for the hybrid estimate. A second limitation is in the convergence accuracy during the optimization of the wave function.

Because the optimization is done in the presence of statistical noise, it is not possible to converge the total energy to a very high precision, which results in some bias in the optimized parameters. Reducing the energy convergence threshold from 10^{-4} Ha to 10^{-3} Ha introduces a random bias on the dipole moment in VMC and to a less extend in DMC which is clearly larger than the statistical uncertainty, but does not change the hybrid estimate within statistical uncertainty. A third limitation is the chosen form of the trial wave function and variational space. Reducing the one-electron basis from CVB2 to CVB1[24] biases the dipole moment in VMC and to a less extent in DMC, but does not change the hybrid estimate. The same behavior is obtained if only the Jastrow parameters are optimized while keeping the CSF and orbital coefficients fixed to their MCSCF values.

C. Results

For any given fragment, the MRCISD and QMC calculations give dipole moments that coincide on the interval of variation considered around the equilibrium positions (see Figure 3). However, the variation of the dipole moment is different in each case. As the CH distance (equivalent to the normal coordinate in this case) increases, one observes:
i) a net decrease of the dipole moment function for the neutral CH($^2\Pi$) fragment consistent with a large IR intensity
ii) a perfect stability of the dipole moment function for the positive ion $CH^+(^1\Sigma^+)$ fragment consistent with a very weak IR intensity
iii) a large increase of the dipole moment function for the positive ion $CH^+(^3\Pi)$ fragment consistent with a large IR intensity.
The B3LYP calculations reported for comparison show the same evolution as the high level treatments, even if the numerical values may vary with the level of theory[11]. Assuming a linear fit over the interval of CH elongation considered, one obtains slope coefficients (Debye/Å) of:

i) CH($^2\Pi$): -1.77(B3LYP); -1.77(MRCI); -1.68(QMC)
ii) $CH^+(^1\Sigma^+)$: 0.18(B3LYP); 0.23(MRCI); 0.22(QMC)
iii) $CH^+(^3\Pi)$: 2.61(B3LYP); 2.56(MRCI); 2.50(QMC),
which justifies the use of the B3LYP density for the topological analysis presented below.

All these calculations are consistent with the fact that the collapse in the IR intensity is linked to the absence of an electron in the π system and not to ionization only.

III. TOPOLOGICAL ANALYSIS

We have represented in Figure 2 a schematic view of the valence electronic distributions in the CH and CH^+ fragments. All three structures are characterized by a covalent CH bond. The differences lie in the repartition of the non bonding electrons between the σ and π orbitals.

The topological analysis carried out in this work relies on a partitioning of the molec-

ular space achieved by means of the theory of dynamical systems[46]. This method gives a mathematical framework enabling a partition of the 3-dimensional physical space into a set of volumes (regions so-called basins and noted Ω). Such a topological analysis has already been successfully used within the QTAIM formalism[47] for which the basins are localized around the atomic centers(QTAIM atoms). Another relevant partition is the topology of the Electron Localization Function hereafter referred to as ELF[48,49]. ELF can be interpreted as a signature of the electronic pairs distributions[50] and it is commonly used in the studies of chemical bonding or chemical reactivity[51–53]. Its topological analysis gives a partition into chemically intuitive regions fulfilling as well as possible a one to one correspondence with the Lewis valence theory: core basins (labelled C(A) around an A atom) contain electrons that are not involved in the chemical bonds and valence basins for lone-pairs (labelled V(A)) and bonding regions (labelled V(A, B)).

Briefly, the population (QTAIM or ELF) of a given basin, noted $N(\Omega)$, is calculated by integrating the charge density over the basin volume[54]. The atomic charge is then calculated for a QTAIM atom according to: $q(\Omega) = \mathrm{Z} - N(\Omega)$. The overlap between the valence orbitals and the basins volumes provides useful information as to the contributions of each orbital to the different basins. In addition, the topological partition makes it possible computing the diffuse character of the electron density distributed into the basin volumes (QTAIM or ELF)[55]. It shows up in the form of intra-atomic dipoles $\mathbf{M}_1$ defined by three-dimensional integrals for a given basin volume according to:

$$\mathbf{M}_1(\Omega) = \int_\Omega (\mathbf{r} - \mathbf{R}_c)\rho(\mathbf{r})d\mathbf{r} \tag{5}$$

where $\mathbf{R}_c$ are the cartesian coordinates of the basin center. In the atoms, the electron density is spherically distributed and consequently, $\mathbf{M}_1$ collapses to zero. This quantity is directly related to the molecular dipole as follows:

$$\boldsymbol{\mu} = \boldsymbol{\mu}^n + \boldsymbol{\mu}^e = [\boldsymbol{\mu}^n - \sum_\Omega N(\Omega)\mathbf{R}_c] + \sum_\Omega \mathbf{M}_1 \tag{6}$$

$$= \sum_\Omega q(\Omega)\mathbf{R}_c + \sum_\Omega \mathbf{M}_1 \tag{7}$$

$$\tag{8}$$

where the first summation is the charge transfer contribution (CT), $q(\Omega)$ being the atomic

charge of a QTAIM atom. The ELF topological analysis and QTAIM analysis presented here were performed via additional calculations using the TopMod package[54,55].

The ELF localisation domains of the $CH(^2\Pi)$, $CH^+(^1\Sigma^+)$ and $CH^+(^3\Pi)$ optimized structures are displayed on the left side of Figure 4 at the B3LYP/Aug-cc-pVTZ level of theory. There is only one core basin C(C), containing two electrons, tightly bound to the carbon nucleus and two valence basins, the first corresponding to the valence electrons non engaged in bonding V(C), the second to the CH bond basin V(C, H). How the dipole moments vary with the elongation of the CH bond around the equilibrium distance is presented in Table 1 that shows the ELF populations and the QTAIM charges and moments for a C-H distance varying between 1.0 and 1.25Å(1.89 to 2.36 a.u.).

1. The neutral fragment CH($^2\Pi$)

There is an increase in the population of the V(C) basin (from 2.84e to 2.92e) coupled to a simultaneous reduction of the V(C, H) basin population (from 2.07e to 2.01e) with the stretching of the CH distance. As the CH bond extends, the contribution N_π of the π electrons to the population of the V(C) basin increases and tends to the value of 1 that will be reached effectively at the dissociation limit. The atomic charges are close to zero and the intra-atomic polarizations $\mathbf{M}_1$(C) and $\mathbf{M}_1$(H) of the two atoms decrease by $\sim$ 50% showing that their electronic densities tend to spherical distributions. The CT charge transfer remains small compared with the total atomic polarization $\mathbf{M}_1$(C+H) whose net decrease is the main reason for the decrease of the dipole moment as each atom, respectively charged $C^{+\delta}$ and $H^{-\delta}$ in the fragment, tends to recover its independence and neutrality.

2. The positive ion fragment $CH^+(^1\Sigma^+)$

There is no change in the populations of the V(C) and V(C, H) with the elongation of the CH bond, both remaining close to two electrons. Contrary to $CH(^2\Pi)$, there is no σ to π electron transfer inside the V(C) basin. The total atomic polarization $\mathbf{M}_1$(C+H) in $CH^+(^1\Sigma^+)$ decreases as strongly as in $CH(^2\Pi)$. However, contrary to the preceding case, it is almost exactly balanced by the rise of the CT contribution. The key result is that the dipole moment does not vary with the C-H distance before the charge is effectively localized

on C.

3. The positive ion fragment $CH^+(^3\Pi)$

There is a net electron transfer from the V(C, H) basin to the σ component N_σ of the carbon V(C) basin with the lengthening of the CH distance. As observed for the previous ion, the CT charge transfer increases, but at the same time there is an increase of the $\mathbf{M}_1$(C+H) total intra-atomic polarization. The increasing distortion of the electronic density with the CH elongation is opposite to that in the two preceding situations. It comes from the fact that this density is submitted to an increasing positive charge on the hydrogen atom. Since there is a simultaneous increase in the CT charge transfer, the dipole moment increases sharply due to this cumulative effect.

IV. CONCLUDING REMARKS

The main goal of this article was to trace the origin of the collapse of the CH vibration with ionization as it shows in the IR spectra of PAHs. Two different approaches have been used to probe the dipole moment functions of the neutral and ionized CH fragment in the vicinity of the equilibrium geometries. The two different approaches, based on "state of the art" ab-initio (MRCISD) and quantum Monte Carlo (QMC) methodologies, converge on the same dipole moment functions for each of the $CH(^2\Pi)$, $CH^+(^1\Sigma^+)$ and $CH^+(^3\Pi)$ electronic states. This result rules out any bias or possible artifact.

Both series of calculations show a strong variation of the dipole moment of $CH(^2\Pi)$, no variation for $CH^+(^1\Sigma^+)$. This result is entirely consistent with the strong and very weak (or non observable) bands of the neutral and ionized PAHs respectively. However, the case of $CH^+(^3\Pi)$ for which there is a very strong variation of the dipole moment demonstrates that ionization is not the determining factor. The key point is the presence, or not, of a hole in the π system. In addition, it is worth stressing the fact that the DFT dipole moment calculated using the B3LYP hybrid functional follows identical variations.

The topological analysis of the B3LYP density using the ELF method shows that the variation of the dipole moment is determined by the relative weights of the two contributions i) the distortion of the intra-atomic densities, and ii) the charge transfer contribution, with

the change in the CH bond length. The compensation of these two effects in $CH^+(^1\Sigma^+)$ is at the origin of the exceptional stability of the dipole moment which in turn is the reason of the observed collapse of the CH stretching vibration.

The present interpretative model should make it possible to predict the strength of the 3.3 μm band according to the electronic structure and type of any neutral or ionized PAHs .

ACKNOWLEDGMENTS

The authors would like to acknowledge fruitful discussions with B. Silvi and R. Assaraf. This work was supported by CNRS national program PCMI (Physics and Chemistry of the Interstellar Medium). Part of the calculations was performed using HPC resources from GENCI-CINES (Grant 2009-085128).

REFERENCES

[1]A. Léger and J. L. Puget, Astron. Astrophys. **137**, L5 (1984).

[2]L. J. Allamandola, A. G. Tielens and J. R. Barker, Astrophys. J. Lett. **290**, L25 (1985).

[3]F. Pauzat, D. Talbi M. D. Miller D. J. DeFrees and Y. Ellinger, J. Phys. Chem. **96**, 7882 (1992).

[4]J. Szczepanski, W. Personette, D. Roser, M. Eyring, R. Pellow and M. Vala, J. Phys. Chem. **96**, 7876 (1992).

[5]D. J. DeFrees, M. D. Miller, D. Talbi, F. Pauzat and Y. Ellinger, Astrophys. J. **408**, 530 (1993).

[6]J. Szczepanski, M. Vala, D. Talbi, O. Parisel, and Y. Ellinger, J. Chem. Phys. **98**, 4494 (1993).

[7]M. Vala, J. Szczepanski, F. Pauzat, O. Parisel, D. Talbi, and Y. Ellinger, J. Phys. Chem. **98**, 9187 (1994).

[8]D. M. Hudgins S. A. Sandford and L. J. Allamandola, J. Phys. Chem. **98**, 4243 (1994).

[9]D. M. Hudgins and L. J. Allamandola, J. Phys. Chem. **99**, 3033 (1995).

[10]S. R. Langhoff, J. Phys. Chem. **100**, 2819 (1996).

[11]C. W. Bauschlicher and S. R. Langhoff, Spectrochim. Acta A **53**, 1225 (1997).

[12]G. Malloci, C. Joblin and G. Mulas, Chem. Phys. **332**, 353 (2007) http://astrochemistry.ca.astro.it/database/ and http://www.cesr.fr/ joblin/database/.

[13]C. Boersma, L. J. Allamandola, C. W. Bauschlicher, A. Ricca, J. Cami, E. Peeters, F. Sanchez, G. Puerto, A. L. Mattioda and D. M. Hudgins, http://www.astrochem.org/pahdb/.

[14]G. Mulas, Astron. Astrophys. **338**, 243 (1998).

[15]O. Pirali, M. Vervloet, G. Mulas, G. Malloci and C. Joblin, Phys. Chem. Chem. Phys. **11**, 3443 (2009).

[16]A. Pathak and S. Rastogi, Spectrochim. Acta A **67**, 898 (2007).

[17]M. Basire, P. Parneix, F. Calvo, T. Pino and Ph. Brechignac, J. Phys. Chem. A. **113**, 6947 (2009).

[18]V. Sivaranjana Reddy and S. Mahapatra, J. Chem. Phys. **128**, 091104 (2008).

[19]V. Sivaranjana Reddy, S. Ghanta and S. Mahapatra, Phys. Rev. Lett. **104**, 111102 (2010).

[20]F. Pauzat and Y. Ellinger, Chem. Phys. **319**, 318 (1997).

[21]M. Jourdain de Muizon, L. d'Hendecourt and T. R. Geballe, Astron. Astrophys. **227**, 526 (1990).

[22]F. Pauzat, D. Talbi and Y. Ellinger, Astron. Astrophys. **319**, 318 (2002).

[23]M. W. Schmidt, K. K. Baldridge, J. A. Boatz, S. T. Elbert, M. S. Gordon, J. H. Jensen, S. Koseki, N. Matsunaga, K. A. Nguyen, S. J. Su, et al., J. Comput. Chem. **14**, 1347 (1993).

[24]I. Ema, J. M. García de la Vega, G. Ramírez, R. López, J. Fernández Rico, H. Meissner and J. Paldus, J. Comput. Chem. **24**, 859 (2003).

[25]W. J. Hehre, R. F. Stewart, and J. A. Pople, J. Chem. Phys. **51**, 2657 (1969).

[26]R. F. Stewart, J. Chem. Phys. **52**, 431 (1970).

[27]R. López, G. Ramírez, J. M. García de la Vega and J. Fernández Rico, J. chim. phys. **84**, 695 (1987).

[28]J. Fernández Rico, G. Ramírez, R. López and J. I. Fernández-Alonso, Collection Czechoslovak Chem. Commun. **53**, 2250 (1988).

[29]A. Kollias, P. Reinhardt, and R. Assaraf, unpublished.

[30]C. J. Umrigar, unpublished.

[31]C. Filippi and C. J. Umrigar, J. Chem. Phys. **105**, 213 (1996).

[32]A. D. Güçlü, G. S. Jeon, C. J. Umrigar, and J. K. Jain, Phys. Rev. B **72**, 205327 (2005).

[33]CHAMP, a quantum Monte Carlo program written by C. J. Umrigar, C. Filippi and J. Toulouse, URL `http://pages.physics.cornell.edu/~cyrus/champ.html`.

[34]J. Toulouse and C. J. Umrigar, J. Chem. Phys. **126**, 084102 (2007).

[35]C. J. Umrigar, J. Toulouse, C. Filippi, S. Sorella, and R. G. Hennig, Phys. Rev. Lett. **98**, 110201 (2007).

[36]J. Toulouse and C. J. Umrigar, J. Chem. Phys. **128**, 174101 (2008).

[37]C. J. Umrigar, Phys. Rev. Lett. **71**, 408 (1993).

[38]C. J. Umrigar, in *Quantum Monte Carlo Methods in Physics and Chemistry*, edited by M. P. Nightingale and C. J. Umrigar (Kluwer, Dordrecht, 1999), NATO ASI Ser. C 525, p. 129.

[39]R. Grimm and R. G. Storer, J. Comput. Phys. **7**, 134 (1971).

[40]J. B. Anderson, J. Chem. Phys. **63**, 1499 (1975).

[41]J. B. Anderson, J. Chem. Phys. **65**, 4121 (1976).

[42]P. J. Reynolds, D. M. Ceperley, B. J. Alder, and W. A. Lester, J. Chem. Phys. **77**, 5593 (1982).

[43]J. W. Moskowitz, K. E. Schmidt, M. A. Lee, and M. H. Kalos, J. Chem. Phys. **77**, 349 (1982).

[44]C. J. Umrigar, M. P. Nightingale, and K. J. Runge, J. Chem. Phys. **99**, 2865 (1993).

[45]J. Toulouse, R. Assaraf, and C. J. Umrigar, J. Chem. Phys. **126**, 244112 (2007).

[46]R. H. Abraham and C. D. Shaw in *Dynamics: The geometry of Behavior*, (Addison Wesley, 1992).

[47]R. F. W. Bader in *Atoms in Molecules: A Quantum Theory (QTAIM)*, (Oxford Univ. Press, Oxford, 1990).

[48]A. D. Becke and K. E. Edgecombe, J. Chem. Phys. **92**, 5397 (1990).

[49]B. Silvi and A. Savin, Nature **371**, 683 (1994).

[50]B. Silvi, J. Phys. Chem. A **107**, 3081 (2003).

[51]B. Silvi, J. Pilmé, F. Fuster and M. E. Alikhani in *Metal-Ligand Interactions*, edited by N. Russo, D. R. Salahub and M. Witko (Kluwer, Dordrecht, 2003), NATO ASI SCIENCES SERIES II:, Mathematics, Physics and Chemistry, p. 241.

[52]J. Poater, M. Daran, M. Solà and B. Silvi, Chem. Rev. **105**, 3911 (2005).

[53]J. P. Piquemal, J. Pilmé, O. Parisel, H. Gérard, I. Fourré, J. Bergès, C. Gourlaouen, A. de la Lande, M. C. van Severen and B. Silvi, Int.J. Quantum Chem. **108**, 1951 (2008).

[54]S. Noury, X. Krokidis, F. Fuster and B. Silvi, Comp. & Chem. **23**, 597 (1999).
[55]J. Pilmé and J. P. Piquemal, J. Comp. Chem. **29**, 1440 (2008).

FIGURES

FIG. 1. Electronic structures of typical PAHs: charge and characteristics of the σ and π electronic distributions. Strengths of the CH stretching vibrations (VS=very strong; vw=very weak) and references.

FIG. 2. Lewis structures of CH in its ground state $^2\Pi$, and CH^+ in its ground state $^1\Sigma^+$ and first excited state $^3\Pi$. In this formal representation, the electrons are distributed in the orbitals following the Hund-Pauli model (Hund's rule for one-center distributions and Pauli principle within a chemical bond).

FIG. 3. Dipole moment of CH in its ground state $^2\Pi$, and CH^+ in its ground state $^1\Sigma^+$ and first excited state $^3\Pi$, with respect to the interatomic distance around the equilibrium, calculated in MRCISD with full core+valence CAS references and in QMC with Jastrow $\times$ full valence CAS wave functions. The QMC results are for the hybrid "2DMC-VMC" estimate and are fitted to quadratic functions, the statistical uncertainties being of the size of the point symbols or smaller.

FIG. 4. ELF localization domains at the equilibrium geometries (left) and at the diabatic dissociation limit (right).

TABLES

TABLE I. Topological analysis in the vicinity of the equilibrium geometries. R_{C-H} is in Å, CT, $\mathbf{M}_1$ and μ are in Debye.

	ELF Populations				QTAIM Analysis						
	V(C)			V(C,H)	C		H		$\sum(C+H)$		
R_{C-H}	N	N_σ	N_π	N	q	$\mathbf{M}_1$	q	$\mathbf{M}_1$	$\mathbf{M}_1$	**CT**	μ
$CH(^2\pi)$											
1.00	2.84	2.11	0.73	2.07	0.03	2.23	-0.03	-0.47	1.76	-0.11	1.65
1.12(eq.)	2.87	2.12	0.75	2.05	0.02	1.75	-0.02	-0.23	1.52	-0.08	1.46
1.14	2.89	2.13	0.76	2.03	0.02	1.70	-0.02	-0.16	1.54	-0.09	1.45
1.18	2.90	2.13	0.77	2.02	0.01	1.54	-0.01	-0.12	1.42	-0.07	1.35
1.25	2.92	2.14	0.78	2.01	0.01	1.46	-0.01	-0.18	1.28	-0.07	1.21
$CH^+(^1\Sigma)$											
1.00	1.97	1.97	0.0	1.99	0.71	1.10	0.29	-0.31	0.79	1.00	1.79
1.14(eq.)	1.96	1.96	0.0	1.98	0.68	0.70	0.32	-0.26	0.44	1.37	1.81
1.18	1.96	1.96	0.0	1.97	0.68	0.61	0.32	-0.23	0.38	1.43	1.81
1.25	1.96	1.96	0.0	1.97	0.68	0.47	0.32	-0.20	0.27	1.56	1.83
$CH^+(^3\Pi)$											
1.00	2.04	1.30	0.74	1.87	0.62	-0.63	0.38	-0.25	-0.88	1.63	0.75
1.14(eq.)	2.16	1.41	0.75	1.76	0.55	-0.84	0.45	-0.20	-1.04	2.14	1.10
1.18	2.22	1.44	0.78	1.70	0.52	-0.90	0.48	-0.19	-1.09	2.29	1.20
1.25	2.32	1.52	0.81	1.61	0.50	-1.02	0.50	-0.15	-1.17	2.57	1.40

I

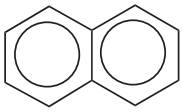

Neutral
Closed shell
σ unsaturation: NO
π hole: NO

I_{CH} = VS

[3, 10]

II

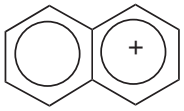

Ionized
Open shell
σ unsaturation: NO
π hole: YES

I_{CH} = vw

[3, 10]

III

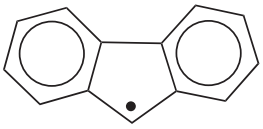

Neutral
Open shell
σ unsaturation: NO
π hole: NO

I_{CH} = VS

[20]

IV

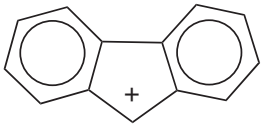

Ionized
Closed shell
σ unsaturation: NO
π hole: YES

I_{CH} = vw

[20]

V

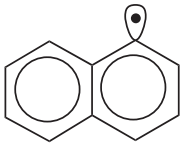

Neutral
Open shell
σ unsaturation: YES
π hole: NO

I_{CH} = VS

[22]

VI

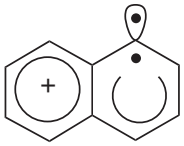

Ionized
Open shell
σ unsaturation: YES
π hole: YES

I_{CH} = vw

[22]

VII

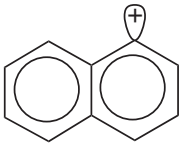

Ionized
Closed shell
σ unsaturation: YES
π hole: NO

I_{CH} = VS

[22]

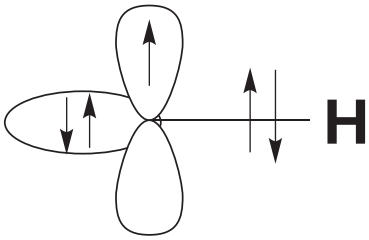

$CH\ (^2\Pi)$

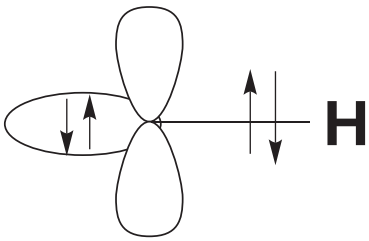

$CH^+\ (^1\Sigma)$

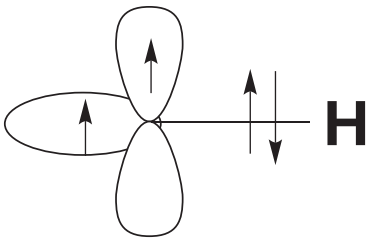

$CH^+\ (^3\Pi)$

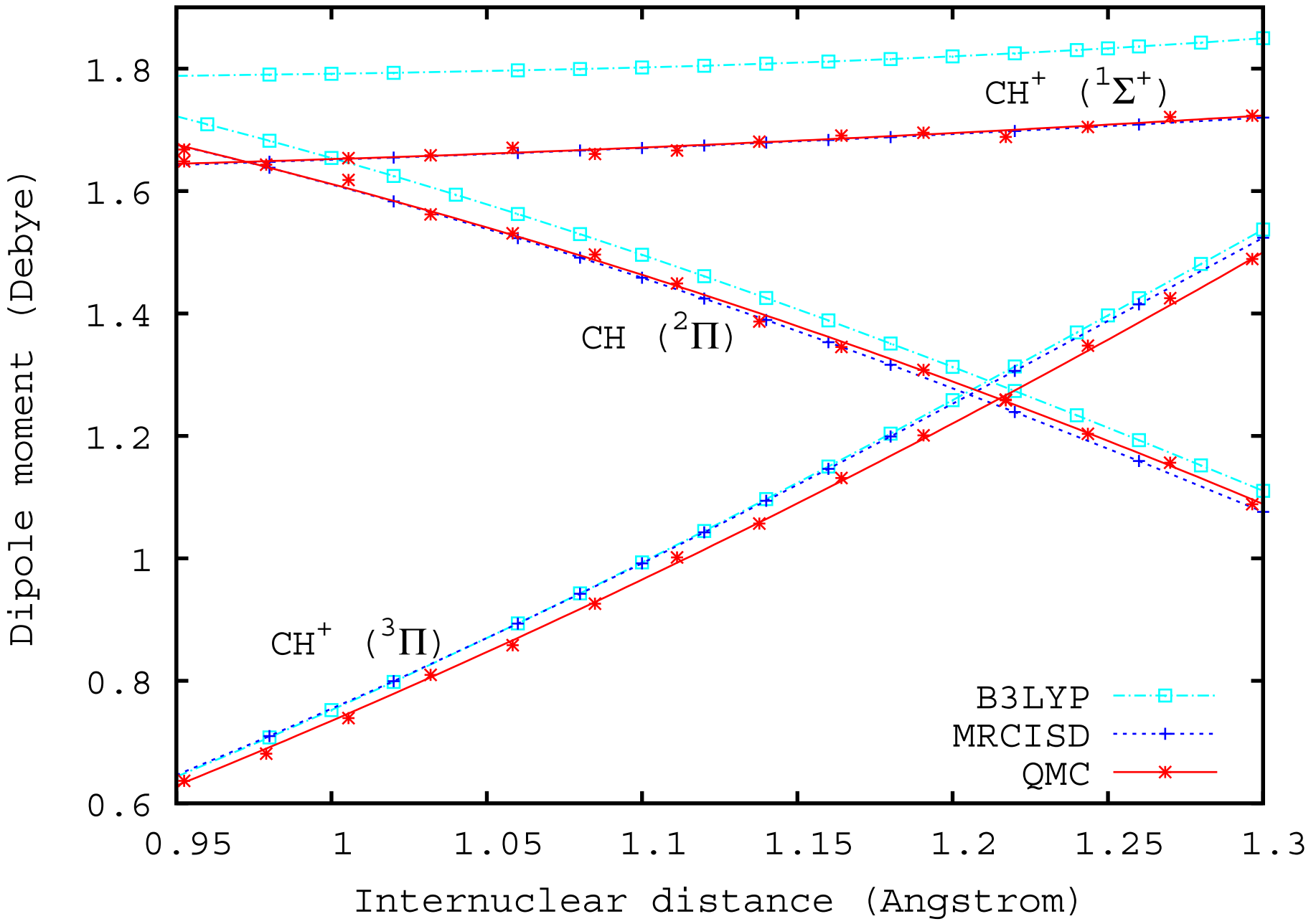
Dipole moment (Debye)
Internuclear distance (Angstrom)
0.6
0.8
1
1.2
1.4
1.6
1.8
0.95
1
1.05
1.1
1.15
1.2
1.25
1.3
CH+ (1Σ+)
CH (2Π)
CH+ (3Π)
B3LYP
MRCISD
QMC

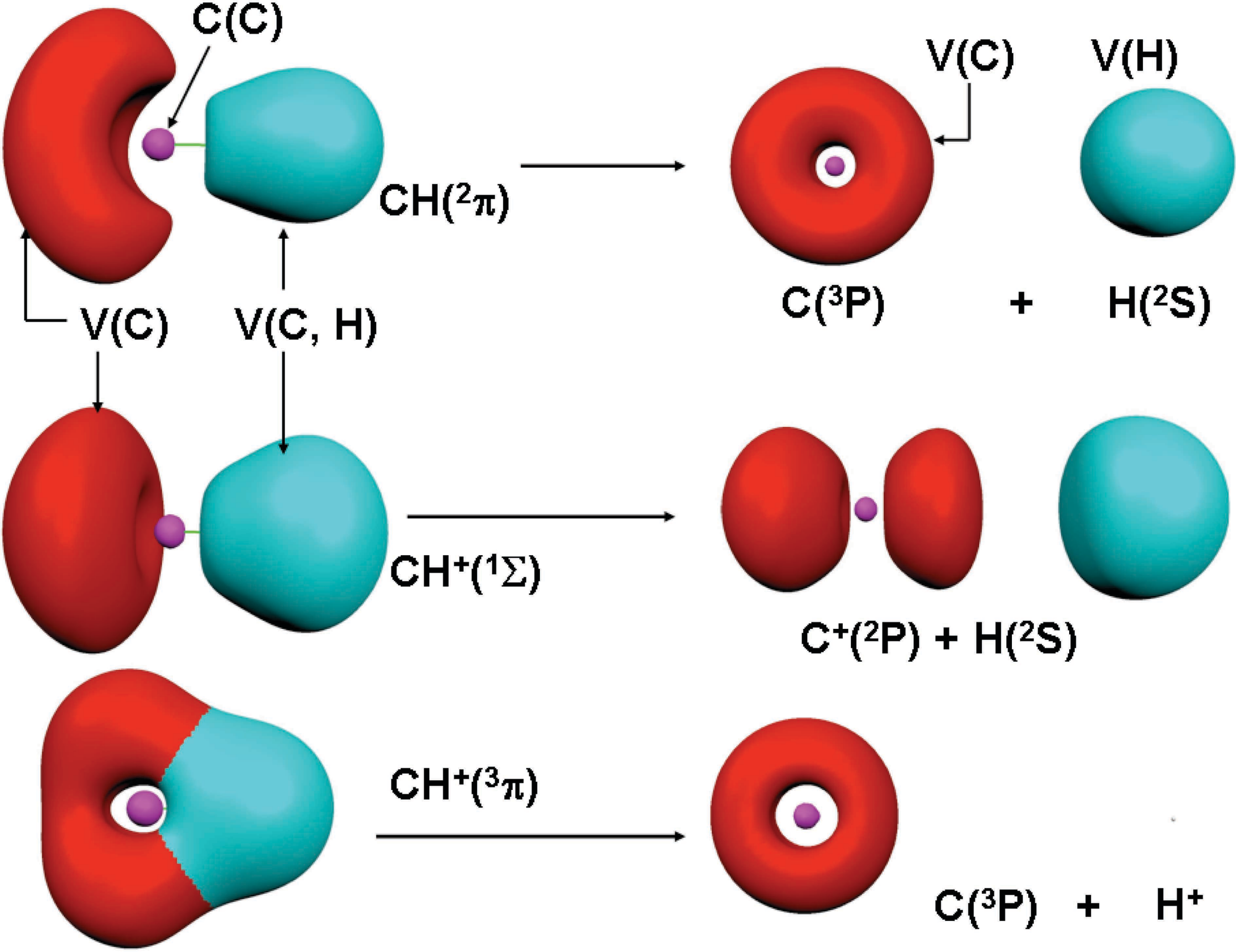
C(C)
CH(²π)
V(C)
V(H)
C(³P) + H(²S)
V(C)
V(C, H)
CH⁺(¹Σ)
C⁺(²P) + H(²S)
CH⁺(³π)
C(³P) + H⁺